doi:10.1088/1742-6596/2647/11/112001

# Higher-order moment stability of large wind turbine blades under stochastic perturbations

## Luca Caracoglia

Department of Civil and Environmental Engineering, Northeastern University, 360 Huntington Avenue, Boston, MA 02115, USA

E-mail: lucac@coe.neu.edu

**Abstract.** The current trend in offshore wind energy is to design and install systems with larger swept areas that yield unprecedented efficiency. Long and slender blades are needed to achieve this objective. As a result of aerodynamic and structural tailoring, slender blades are particularly susceptible to various dynamic instability phenomena during standard operations. One of these phenomena is the bending-torsion flutter that may lead either to structural failure or system breakdown. The research author has been examining blade flutter under the influence of stochastic perturbations, which include both flow turbulence and aeroelastic load variability.

A reduced-order Markov model has been used to describe the effects of the various random perturbations. Mean-square stability has been recently explored; results suggest that perturbations may negatively impact the flutter angular speed and increase the risk of failure.

In this study the model is employed to investigate moment stability beyond mean squares, observing that dynamic instability involves nonlinear propagation of the perturbations and may exhibit amplitude dependency. Third-order instability is investigated and compared against previous numerical results. The NREL 5MW reference wind turbine blade is used as a benchmark example.

## 1. Introduction and study objectives

Offshore wind energy requires large swept areas to increase energy production. Future turbines will have blades of length 100 m or more (e.g., [1]). A large blade radius increases the sensitivity to flow-induced instability, which may be influenced by various random perturbations. Flow-induced instability of wind turbine blades has been noted by various researchers [1, 2, 3, 4, 5, 6]. Among the various types of instability, classical flutter is possible at small angles of attack if attached-flow conditions are present around the blade. Classical flutter predominantly entails coupling between a torsional blade mode and a flapwise mode. Traditionally, issues have been avoided in wind turbine blades either because the rotor's operational angular speeds are low or the blades are stiff (e.g., [2]). Nevertheless, modern blades are slender, more sensitive and with a small ratio between torsional and flapwise frequencies of the two leading modes that control flutter [7, 8]. Coupled-mode flutter is possible at a critical angular speed close to the operational angular speeds of the wind turbine [9]. This problem can negatively affect the structural reliability of the blade.

The main study motivation is related to the preeminence of estimation errors in the blade structural properties and aeroelastic loads, as identified by the research community [10, 11]. Nevertheless, the blade flutter problem has been mainly studied by neglecting the effect of flow

Content from this work may be used under the terms of the Creative Commons Attribution 4.0 licence. Any further distribution of this work must maintain attribution to the author(s) and the title of the work, journal citation and DOI.

doi:10.1088/1742-6596/2647/11/112001

turbulence, even though this condition has been investigated in other structures, such as long-span bridges [12, 13, 14, 15, 16, 17] and rotorcrafts [18, 19]. The probability of blade flutter is examined through an implementation of stochastic differential equations [20]. The specific study objectives are to:

- (i) derive a flow field formulation that incorporates stationary turbulence;
- (ii) use a rotationally sampled spectrum to describe inflow turbulence [21, 22];
- (iii) account for relative mean inflow velocity, noting that the relative tangential velocity component, due to blade rotation in the rotor plane, is large compared to the mean inflow wind speed, orthogonal to the rotor plane;
- (iv) explore moment stability [23, 24] beyond mean squares, already examined by the author [25, 26], by accounting for various perturbations.

The rotationally-sampled turbulence spectrum is converted to dimensionless time via autoregressive filter that operates on a standard Wiener noise. A reduced-order model is constructed to simulate the blade dynamics, with state vector incorporating both the turbulence variable and the "aeroelastic states". The weak solution of the stochastic differential equations is studied [27], i.e., through repeated sampling and numerical integration of each realization. The National Renewable Energy Laboratory (NREL) 5-MW offshore wind turbine blade is used as a benchmark example [9] since it has been demonstrated [4, 28] that this blade is susceptible to flutter.

# 2. Theoretical background

#### 2.1. Turbulence perturbations in the rotor plane

Figure 1 illustrates the rotor-plane, dimensional turbulence component  $u(x, \phi; t)$  that combines vertical turbulence w and across-wind, horizontal turbulence v components over time t.

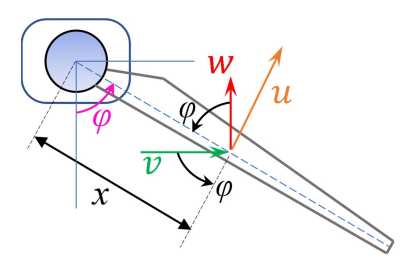


**Figure 1.** Rotor-plane turbulence u defined by vector summation of vertical w and across-wind v turbulence, with "frozen" azimuth angle  $\varphi$ .

The relevant turbulence component is w since the vertical and across-wind terms, along with dependence on azimuth angle  $\varphi$  are less important. Spatial, lengthwise loss of correlation is neglected. Consequently, rotor-plane tangential turbulence field is homogeneous with  $u(x,t) \approx u(t) \approx w(t)$ , and conservatively behaves as a fully correlated gust on the blade. Future developments may consider a more refined field in the lengthwise direction.

The blade has length R and rotates with angular speed  $\Omega$ . The spectrum of the stationary, zero-mean w is simulated by one-sided Lumley-Panofsky power spectral density (PSD) of w [29] and transformed to two-sided dimensionless spectrum of  $w_{\texttt{ND}} = w/(\Omega R)$  for a fixed point at the rotor center:

$$S_{w_{\text{ND}}} = 0.5 \frac{33.6u_{*}^{2}}{\left[1 + 10k_{*}^{5/3} \left(\frac{\omega_{0j}H}{2\pi \bar{U}_{H}}\right)^{5/3}\right]}$$
(1)

doi:10.1088/1742-6596/2647/11/112001

In Eq. (1) the dimensionless frequency is  $k_* = \omega/\omega_{0j}$  with  $\omega_{0j}$  being the angular frequency of the reference flapwise mode j;  $\bar{U}_H$  is the mean wind speed at hub height H;  $u_*$  is the friction velocity of the boundary layer. The turbulent flow is seen by an observer standing on a generic blade cross section at x from rotor center while blade rotates with angular speed  $\Omega$  (Fig. 2). The energy of fixed-point spectrum in Eq. 1 is perturbed by blade rotation (advancing or delaying the free field gusts). The energy is re-distributed from low frequencies to higher frequencies. This rotationally sampled spectrum gives rise to concentrations of PSD at multiples of the frequency corresponding to the angular speed  $\Omega$ . The first "spike" coincides with frequency 1P of the blade,  $k_* = \chi = \Omega/\omega_{0j}$  in dimensionless units. A method based on the principle of second-order auto-regressive filters (AR-2) is employed to describe this phenomenon [25]. After Fourier analysis, the AR-2 dimensionless turbulence is relabeled as  $u_{\Omega}$  and found as [25]

$$S_{u_{\Omega}} = \frac{S_{w_{\text{ND}}}(k_{*})}{T_{1,\text{ND}}k_{*}^{2} + (T_{2,\text{ND}} - T_{3,\text{ND}}k_{*}^{2})}$$
(2)

In Eq. (2) the coefficients  $T_{1,\text{ND}}$ ,  $T_{2,\text{ND}}$ ,  $T_{3,\text{ND}}$  can be aptly calibrated. The filtered, dimensionless turbulence spectrum in Eq. (2) depends on the spectrum of Eq. (1). The energy of background (bk), rotationally sampled turbulence can be related to total energy of the unfiltered spectrum through mean squares as  $\sigma_{u_{\Omega,\text{bk}}}^2 = \Upsilon_{\text{bk}}\sigma_{w_{\text{ND}}}^2$ , i.e.,  $T_{2,\text{ND}} = \Upsilon_{\text{bk}}^{-1/2}$ ; the resonant peak occurs at  $k_* = \chi = \Omega/\omega_{0j}$  and leads to  $T_{3,\text{ND}} \approx \Upsilon_{\text{bk}}^{-1/2}\chi^{-2}$ ; the ratio between peak resonant spectrum and background spectrum can be defined using an amplification factor  $\Upsilon_{\text{amp}}$  that depends on the radial position from the rotor center [22] and yields to  $T_{1,\text{ND}} = \Upsilon_{\text{amp}}^{-1}\chi^{-2}$ .

## 2.2. Dynamic model: foreword

Fig. 2 illustrates a wind turbine blade of radius R, rotating at an angular speed  $\Omega$  (rad/s). The mean flow conditions in the rotor plane are also displayed. A typical blade cross section is located at a distance x from the rotor center. The in-plane, tangential inflow speed linearly varies along the x axis. Furthermore, the chord length of the blade's section varies along x, i.e., it is tapered. Standard flutter theory cannot be used. The model assumptions are:

- linear elastic beam model [30] rotating at angular speed  $\Omega$ ;
- response is described by modal superposition and coupling of one flapwise (jth) and one torsional mode (kth) with angular frequencies  $\omega_{0j}$  and  $\omega_{0k}$ , respectively;
- edgewise blade motion and initial twist angle are not considered;
- small vibration amplitude is examined at incipient instability;
- mean in-plane flow speed at x from hub is  $U(x) \approx \Omega x$  [4];
- mean flow is perturbed by a homogeneous, rotor-plane (or in-plane) turbulence field  $u(x,t) \approx w(t)$ , acting conservatively as a fully correlated gust along blade axis;
- unsteady theory of aeroelastic loads is employed.

The hypothesis  $U(x) \approx \Omega x$  [4] is adequate since the mean, relative velocity component in the rotor plane is of the order of  $\Omega R \approx 70 \,\text{m/s}$  at blade free-end, compared to the mean wind speed, orthogonal to the rotor plane, which is about 12 m/s [9].

Flutter involves coupling of two primary structural modes [7, 31]. The relevant modes are one fundamental flap-wise (mode j) and one torsional (mode k). The dynamic equations are therefore expressed using blade's flapwise deflections  $h(\tau, \eta) \approx \xi_j(\tau)c_0h_j(\eta)$  and torsional rotations  $\alpha(\tau, \eta) = \xi_k(\tau)c_0\alpha_k(\eta)$  with generalized coordinates  $\xi_j(\tau)$  and  $\xi_k(\tau)$ , respectively;  $c_0$  is a reference (root) blade chord length,  $h_j(\eta)$  and  $\alpha(\eta)$  are dimensionless mode shape functions. The time is dimensionless  $\tau = t\omega_{0j}$  and the spanwise sectional coordinate (Fig. 2) is  $\eta = x/R$ .

doi:10.1088/1742-6596/2647/11/112001

After simplifications, the dimensionless, two-mode, generalized blade equations are, with prime symbol designating derivative with respect to  $\tau$ :

$$\xi_j''(\tau) + 2\zeta_j \xi_j'(\tau) + \xi_j(\tau) + \epsilon_j \chi^2 \xi_j(\tau) = \frac{Q_j(\tau)}{\omega_{0j}^2 I_{0j}}$$
(3)

$$\xi_k''(\tau) + 2\zeta_k \Delta \omega \xi_k'(\tau) + (\Delta \omega)^2 \xi_k(\tau) + \epsilon_k \chi^2 \xi_k(\tau) = \frac{Q_k(\tau)}{\omega_{0j}^2 I_{0k}}$$
(4)

In Eq. (3) the flap-wise mode j is the reference one. The flutter frequency ratio is  $\chi = \Omega/\omega_{0j}$ ; the modal frequency ratio is  $\Delta\omega = \omega_{0k}/\omega_{0j}$ ; coefficients  $\epsilon_j$  and  $\epsilon_k$  account for the centrifugal forces on the rotating blade;  $\zeta_{0j}$  and  $\zeta_{0k}$  are modal damping ratios.  $I_{0j}$  and  $I_{0k}$  are generalized modal inertias [1]. In Eq. (3) and in Eq. (4) the generalized forces  $Q_j$  and  $Q_k$  are adapted from unsteady aeroelastic theory of airfoils via indicial functions to describe non-circulatory flow effects. As demonstrated in [25] the standard indicial Wagner function [7], traditionally used for blade aeroelasticity [5, 32] cannot be used since the chord length and tangential velocity U(x) vary along x in Fig. 2. Therefore, the Wagner function is expressed in terms of  $\tau$  and by Taylor series of order N [25].

# 2.3. Stochastic model accounting for turbulence perturbations

The formulation by Jones [33] with  $\Phi_0 = \Phi(0) = 1 - (c_1 + c_2)$  is used to represent the Wagner function; the standard equation reads  $\Phi(s) = 1 - \sum_{r=1}^2 c_r e^{-d_r s}$  with time s and parameters  $c_r$ ,  $d_r$  ( $r = \{1, 2\}$ ). If rotor-plane tangential turbulence  $u(\tau) = u_\Omega \Omega R$  (Section 2.1) is considered, the relative, instantaneous squared inflow velocity of the aerodynamic load model is  $[-U(\eta) + u(\eta, \tau)]^2 \approx U^2(\eta) - 2U(\eta)u(\tau)$  in dimensional units  $[m/s^2]$ . The corresponding generalized load term proportional to  $2U(\eta)u(\tau)$  is attributed to circulatory flow effects. The wind gust, generating the load perturbation, is fully correlated along the blade length.

The generalized forces can be aptly derived, e.g., the generalized force  $Q_j$  of mode j is:

$$\begin{split} \frac{Q_{j}(\tau)}{\omega_{0j}^{2}I_{0j}} &= \Gamma_{j}^{\text{C}}C_{L}^{*}\chi^{2} \Biggl\{ \frac{\Phi_{0}c_{0}}{2R\chi} \left[ G_{h_{j}h_{j}}^{(-1)} - u_{\Omega}G_{u,h_{j}h_{j}}^{(-1)} \right] \xi_{j}' + \Phi_{0} \left[ G_{h_{j}\alpha_{k}}^{(0)} - u_{\Omega}G_{u,h_{j}\alpha_{k}}^{(0)} \right] \xi_{k}' \\ &+ \sum_{n=0}^{N} \left[ \frac{1}{n!} \left( \frac{2R\chi}{c_{0}} \right)^{n} \left[ c_{1}d_{1}^{n+1} + c_{2}d_{2}^{n+1} \right] \left[ G_{h_{j}h_{j}}^{(n)} - u_{\Omega}G_{u,h_{j}h_{j}}^{(n)} \hat{\eta}_{ae,j}^{(n)} \right] \right] \\ &+ \sum_{n=0}^{N} \left[ \frac{1}{n!} \left( \frac{2R\chi}{c_{0}} \right)^{n} \left[ c_{1}d_{1}^{n+1} + c_{2}d_{2}^{n+1} \right] \left[ G_{h_{j}\alpha_{k}}^{(n+1)} - u_{\Omega}G_{u,h_{j}\alpha_{k}}^{(n+1)} \hat{\nu}_{ae,j}^{(n)} \right] \right] \right\} \\ &\Gamma_{j}^{\text{NC}} \left\{ G_{h_{j}h_{j}}^{(-1)} \xi_{j}'' + R\chi c_{0}^{-1}G_{h_{j}\alpha_{k}}^{(-1)} \xi_{k}' - \frac{a}{2}G_{h_{j}\alpha_{k}}^{(m)} \xi_{k}'' \right\} \end{split}$$

In Eq. (5)  $C_L^*$  is the derivative of the lift coefficient with respect to the static angle of attack, evaluated at angle 0 [28]. Quantities  $\Gamma_j^{\text{C}}$  and  $\Gamma_j^{\text{NC}}$  are dimensionless modal inertias. The quantities  $\hat{\eta}_{ae,j}^{(n)}$  and  $\hat{\nu}_{ae,j}^{(n)}$  on the second and fourth line of Eq. (5) are partial aeroelastic states [25]. The dimensionless parameter a (normalized with respect to  $c_0/2$ ) on the fifth line of Eq. (5) measures the offset between the center of mass and the center of stiffness of the blade from a generalized model perspective. The modal integrals  $G_{h_j\alpha_k}^{(n)}$  of the circulatory flow component (with index  $n=\{-1,0,1,\ldots,N\}$ ),  $G_{u,h_j\alpha_k}^{(n)}$  and  $G_{h_j\alpha_k}^{(m)}$  of the non-circulatory term (superscript with no index) are described in [25, 26] and are not presented herein for the sake of brevity.

doi:10.1088/1742-6596/2647/11/112001

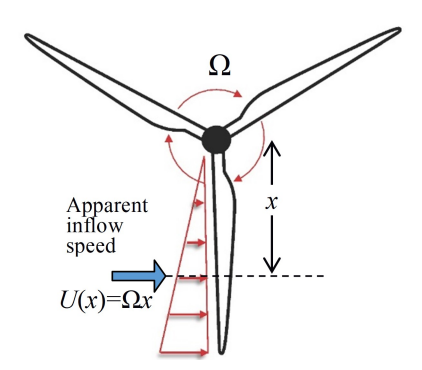


**Figure 2.** Rotating wind turbine blade with mean, in-plane velocity U(x) and  $0 \le x \le R$ .

Eqs. (3),(4),(5) are transformed to Itô-type stochastic differential equation [20], by expressing the random turbulence  $w_{ND}$  in Eq. (1) as output to a 1st-order autoregressive filter (AR-1):

$$dw_{ND} = -G_{1,w_{ND}}d\tau + G_{2,w_{ND}}dB(\tau)$$
(6)

In Eq. (6)  $B(\tau)$  is a dimensionless, scalar Wiener process of unit-variance independent Gaussian increments [20]. The parameters of this equation can be found by least squares fitting of Eq. (1); Fourier analysis of Eq. (6) yields a two-sided spectrum  $S_{w_{\rm ND}} \approx G_{2,w_{\rm ND}}^2/(k_*^2 + G_{1,w_{\rm ND}}^2)$ . Subsequently, the random variable of the state vector  $w_{\rm ND}$  is filtered by the AR-2 filter with spectrum in Eq. (2), which is rewritten as a second-order linear differential equation that includes two new input variables,  $u_{\Omega}$  and  $du_{\Omega}/d\tau$ , added to the state vector. The final, stochastic differential equation is:

$$d\mathbf{Z}(\tau) = \mathbf{a}_{NL,w}(\mathbf{Z}(\tau))d\tau + \sqrt{2\pi}\mathbf{d}_w dB(\tau)$$
(7)

In Eq. (7), **Z** is a multi-variable state vector, which includes modal coordinates  $(\xi_j, \xi_k)$ , their first derivatives  $(\mathrm{d}\xi_j/\mathrm{d}\tau, \mathrm{d}\xi_k/\mathrm{d}\tau)$ , partial aeroelastic states  $(\hat{\eta}_{ae,j}^{(n)}, \hat{\nu}_{ae,j}^{(n)})$  and turbulence states  $(u_\Omega, \mathrm{d}u_\Omega/\mathrm{d}\tau, w_{\rm ND})$ . The drift function  $\mathbf{a}_{\rm NL,w}$  is nonlinear because of the parametric turbulence perturbation in Eq. (5), i.e., quadratic cross-terms like  $u_\Omega \xi_k$ . The diffusion vector is  $\mathbf{d}_w = [0, 0, \dots, 0, G_{2,w_{\rm ND}}]^T$ . The "Wong-Zakai" [34] corrections terms are considered.

## 2.4. Stochastic model accounting for aeroelastic load perturbations

Propagation of aeroelastic load uncertainty examines wind tunnel errors and modeling simplifications. In this study aeroelastic load perturbations are treated separately from turbulence. Therefore, Eq. (5) is first simplified to eliminate dependency on turbulence perturbations, i.e., by setting  $u_{\Omega} = 0$ . Instead, the term  $d_2$  on the third and fourth line of Eq. (5) that represents the Wagner function is replaced by  $d_2(\tau) = d_{2,m} + \delta_2(\tau)$ , with  $d_{2,m}$  being the reference or mean value and  $\delta_2(\tau)$  a zero-mean Gaussian time-dependent random error. Equations (3),(4),(5) are again transformed to Itô-type stochastic differential vector equation. A new unit-variance Wiener process  $\tilde{B}(\tau)$  is used to simulate the error propagation. The state vector  $\tilde{\mathbf{Z}}$  is different because it does not include variables related to turbulence but it still includes  $(\xi_j, \xi_k)$ ,  $(d\xi_j/d\tau, d\xi_k/d\tau)$ ,  $(\hat{\eta}_{ae,j}^{(n)}, \hat{\nu}_{ae,j}^{(n)})$  and, most importantly, the added effect of random aeroelastic  $\delta_2(\tau)$ , introduced by state augmentation [20] directly into  $\tilde{\mathbf{Z}}(\tau)$ . This new equation reads:

$$d\tilde{\mathbf{Z}}(\tau) = \mathbf{a}_{\text{NL},\text{ae}}(\tilde{\mathbf{Z}}(\tau))d\tau + \sqrt{2\pi}\mathbf{d}_{\text{ae}}d\tilde{B}(\tau)$$
(8)

In Eq. (8) with a forcing function exclusively aeroelastic and no turbulence, the drift function  $\mathbf{a}_{NL,ae}$  is nonlinear because of  $\delta_2(\tau)$  whereas the diffusion vector  $\mathbf{d}_{ae}$  is zero and so is  $\tilde{B}(\tau)$ : state

doi:10.1088/1742-6596/2647/11/112001

augmentation incorporates the variable  $\delta_2(\tau)$  as a state of  $\tilde{\mathbf{Z}}(\tau)$ . Solving Eq. (8) slightly differs from Eq. (7) in Section 2.3 since drift only controls the deviation from a stable equilibrium. Nevertheless, the procedure is the same and is described in the next sub-section.

## 2.5. Monte-Carlo estimation of Moment Lyapunov Exponents

The stochastic equations Eq. (7)-(8) are solved numerically multiple times with appropriate initial conditions by Euler time-marching solver. Statistical moments are evaluated by Monte Carlo sampling [35]. The pth order Moment Lyapunov Exponent (MLE) is used to examine the stochastic stability, numerically evaluated:

$$\Lambda_{\Xi}(p) \approx \log_{e} \left( \mathbb{E} \left[ \|\Xi(\tau_{l})\|^{p} \right] \right) / \tau_{l} \tag{9}$$

with  $\Xi(\tau_l) = [\xi_j, \xi_k, \mathrm{d}\xi_j/\mathrm{d}\tau, \mathrm{d}\xi_k/\mathrm{d}\tau]^T$  evaluated at discrete time  $\tau_l$ ; time  $\tau_l$  is sufficiently large, i.e., Eq. (9) approximates the limit as  $\tau_l$  tends to infinity;  $\mathbb{E}[.]$  is the expectation operator applied to the pth vector norm of  $\Xi$ . The MLE measures the propensity of the system's slow dynamics to asymptotically exhibit a diverging trend; it is commonly employed for stability of nonlinear stochastic systems [23]. In this work, stability is studied using  $p = \{2, 3\}$  norms. The sample population employed to numerically solve Eq. (9) is set to 400; the dimensionless time step used for integration of Eq. (8) or Eq. (7) is set to  $\Delta \tau = 0.1$ .

## 3. The 5MW NREL benchmark blade problem

The previous remarks and model are applicable to the 5MW NREL wind turbine blade [4, 9]. The coupled-mode flutter of the rotating blade is studied. The blade radius is  $R=61.5\,\mathrm{m}$  and reference chord length is set to  $c_0=3.8\,\mathrm{m}$  at the root section. The hub height is  $H=90\,\mathrm{m}$ . The reduced-order dynamic model utilizes the third flapwise mode j [with frequency  $\omega_{0j}/(2\pi)=4.34\,\mathrm{Hz}$ ] and the first torsional mode k [with frequency  $\omega_{0j}/(2\pi)=5.39\,\mathrm{Hz}$ ]. Modal damping ratios are set to 0.48% for both modes. The dimensionless offset between elastic center and mass center is set to a=-1. The modulus of the static lift slope is  $C_L^*=\pi$  constant along the blade's airfoil cross section, while the slope of the static moment coefficient is  $C_L^*=\pi/2$ . The aeroelastic load parameters are derived from the Wagner function, i.e.,  $c_1=0.165, d_1=0.0455, c_2=0.335, d_2=0.3$ . The centrifugal force effects along the blade axis are accounted for by  $\epsilon_j=\epsilon_k=0.2$  [25].

Fig. 3 shows the rotationally sampled wind turbulence spectrum  $u_{\Omega}$ , designated as "base" turbulence scenario, referenced to angular speed close to flutter (rated speed  $\Omega=12.1\,\mathrm{rpm}$ ). The graph is found from the Panofsky spectrum, approximated as  $S_{w_{\mathrm{ND}}}\approx G_{2,w_{\mathrm{ND}}}^2/(k_*^2+G_{1,w_{\mathrm{ND}}}^2)$ . The spectrum is normalized with respect to reduced frequency  $k_*$  where the mean wind speed orthogonal to the rotor plane at hub height is  $\hat{U}_H=11.4\,\mathrm{m/s}$  that is found by setting the logarithmic law of the boundary layer with roughness length  $z_0=0.005\,\mathrm{m}$  for offshore exposure. The PSD of the rotationally sampled turbulence model is found using the AR-2 model in Fig. (2). The figure also compares the exact Panofsky PSD in Eq. (1) with the approximate spectrum found using Eq. (6).

In the standard scenario, the following parameters are used:  $\Upsilon_{\rm bk} = 70\%$ , derived from the literature [21],  $\Upsilon_{\rm amp} = 4$ , appropriate for medium-sized blades of radius  $R > 30\,\rm m$ . The fitting results yield  $G_{1,w_{\rm ND}} = 8.8 \times 10^{-3}$  and  $G_{2,w_{\rm ND}} = 6.46 \times 10^{-5}$  at rated angular speed. There is a localized peak in the PSD at 1P frequency  $k_* \approx \chi \approx 0.05$ . Contrary to standard PSD, the fitting must be repeated as either  $\Omega$  or  $\chi$  varies. The fitting operates as a filter that captures the main features of the turbulence swept by a rotating blade. However, the fitting does not consider higher-order effects at  $k_* > 0.1$  (2P, etc. [21]), i.e., in the inertial frequency sub-range of the Panofsky spectrum that, for large blades such as the one examined herein, yields negligible dynamic effects only.

doi:10.1088/1742-6596/2647/11/112001

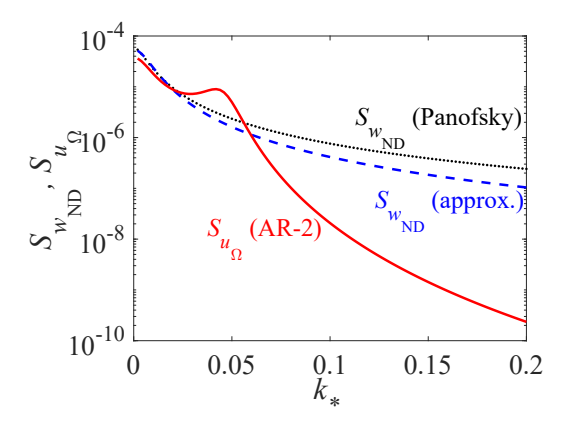


**Figure 3.** Two-sided, dimensionless power spectral density (PSD) of the rotationally sampled flow turbulence surrounding the 5MW NREL wind turbine blade, shown for  $k_* > 0$  only.

Furthermore, a second, enhanced turbulence scenario is considered. In this second scenario  $\sigma_{u_{\Omega}}$  is increased to study influence of intensity:  $\Upsilon_{\rm bk} = 140\%$  is used, while  $\Upsilon_{\rm amp}$ ,  $\hat{U}_H$  are the same as before. A larger  $\Upsilon_{\rm bk}$  simulates an increase in the intensity of background flow turbulence by a factor of  $\sqrt{2}$ . Spectral ordinates of the PSD function are doubled, compared to the values shown in Fig. 3.

#### 4. Stability results

#### 4.1. Deterministic analysis

Deterministic flutter can be examined by computing the system's complex eigenvalues as a function of  $\Omega$  or  $\chi$ , and by locating a zero-damping "modal branch" that triggers instability. Using the information and the reduced-order model, the critical flutter rotor speed is 17.2 rpm from literature [25] vs. 20.7 rpm [4]. The flutter frequency is 4.5 Hz vs. 3.6 Hz. Differences can be explained by noting that flutter of the NREL 5-MW wind turbine blade is partly influenced by the 2nd flapwise mode, yielding a 10% increment of  $\Omega$ . Although addition of a third mode can readily be considered, the current prediction (17.2 rpm) is conservative and, therefore, suggests adequacy of this result for the purposes of this study. Moreover, a constant lift slope  $C_L^*$  is used herein, while it should vary, as noted by previous investigators [4], because of various blade airfoils being used.

# 4.2. Turbulence perturbations

Fig. 4 illustrates the second- and third-moment stochastic stability of the NREL 5-MW wind turbine model, illustrated above, subject to turbulent flow perturbation with moderate intensity (base scenario), the spectrum of which is presented in Fig. 3. The four panels show examples of MLE analysis,  $\Lambda_{\Xi}(2)$  and  $\Lambda_{\Xi}(3)$  at angular rotor speeds  $\Omega=15.49\,\mathrm{rpm}$  (below the deterministic flutter threshold) and  $\Omega=17.18\,\mathrm{rpm}$ . Random initial conditions at  $\tau=0$  are also considered by imposing an initial, random generalized displacement of the flapwise mode j ( $\xi_{0j}$ ) with zero mean and variable variance. The variance  $\mathrm{E}[\xi_{0j}^2]$  describes small, moderate and large (unrealistic) variations.

Examination of Fig. 4 indicates that turbulence is detrimental since both second and third MLEs rapidly diverge to an unstable value [e.g.,  $\Lambda_{\Xi}(2) > 0$  in Fig. 4a or  $\Lambda_{\Xi}(3) > 0$  in Fig. 4c] for  $\tau > 10$  (i.e., as  $\tau \to +\infty$  at  $\Omega = 15.49\,\mathrm{rpm}$ . The two trends  $\Lambda_{\Xi}(2)$  and  $\Lambda_{\Xi}(3)$  are similar, irrespective of initial conditions, and suggest that differentiating between second-moment and third-moment stability appears rather irrelevant to this base turbulence scenario. This result

doi:10.1088/1742-6596/2647/11/112001

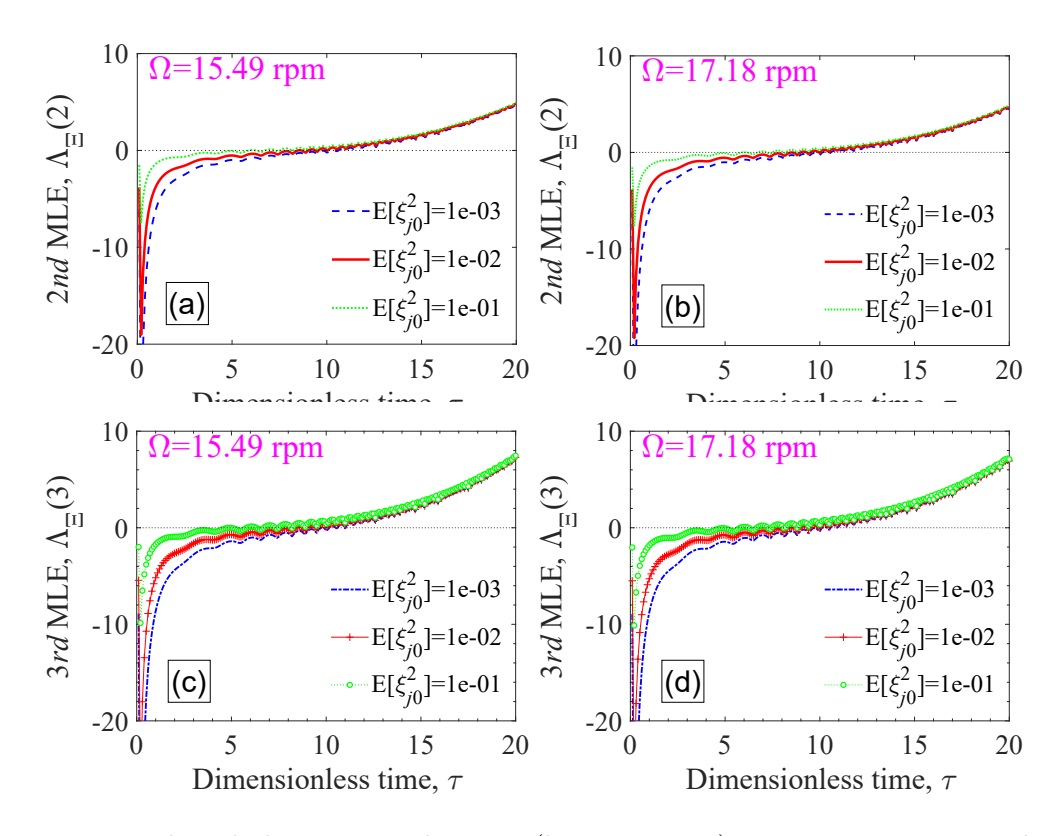


**Figure 4.** Wind turbulence perturbations (base scenario) - NREL 5-MW wind turbine blade stability at various rotor speeds  $\Omega$ : (a) 2nd MLE at  $\Omega = 15.49 \,\mathrm{rpm}$ , (b) 2nd MLE at  $\Omega = 17.18 \,\mathrm{rpm}$ , (c) 3rd MLE at  $\Omega = 15.49 \,\mathrm{rpm}$ , (d) 3rd MLE  $\Omega = 17.18 \,\mathrm{rpm}$ .

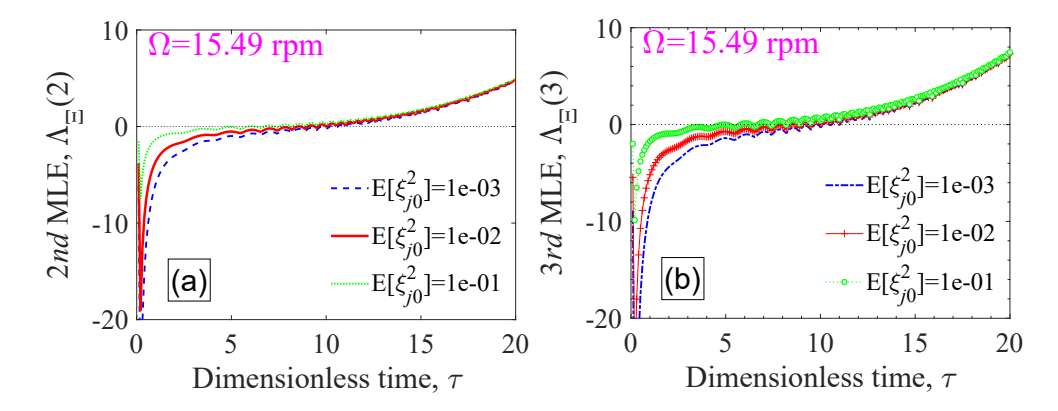


Figure 5. Wind turbulence perturbations (enhanced scenario) - NREL 5-MW wind turbine blade stability at  $\Omega = 15.49 \, \text{rpm}$  rotor speed: (a) 2nd MLE, (b) 3rd MLE.

confirms the findings of a previous study [25]. Fig. 5 depicts the stability results at  $\Omega = 15.49 \,\mathrm{rpm}$  with enhanced turbulence scenario. Difference are almost imperceptible, compared to Fig. 4.

# 4.3. Aeroelastic load perturbations

Fig. 6 illustrates an example of stability analysis associated with aeroelastic load perturbations. In this case, turbulence effects are not included. Eq. (8) is used and solved numerically to find the corresponding MLE values. The load perturbation  $\delta_2(\tau)$  is Gaussian with zero mean and standard deviation  $\sigma_{\delta_2} = 0.022$ , which approximately corresponds to 7.5% coefficient of variation

doi:10.1088/1742-6596/2647/11/112001

for  $d_2 = d_{2,m}$ .

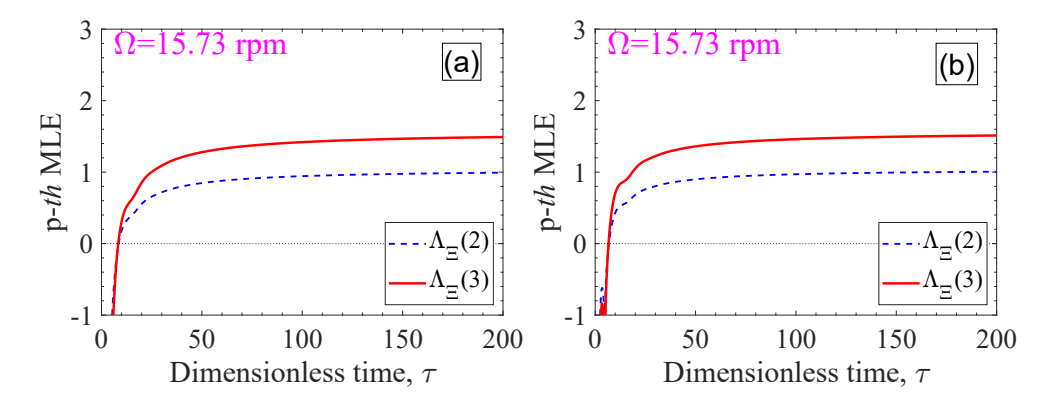


**Figure 6.** Aeroelastic load perturbations - NREL 5-MW wind turbine blade stability at  $\Omega = 15.73$  rpm rotor speed: (a)  $E[\xi_{0i}^2] = 1e - 02$ , (b)  $E[\xi_{0i}^2] = 1e - 01$ .

The figure panels present both  $\Lambda_{\Xi}(2)$  and  $\Lambda_{\Xi}(3)$  at angular rotor speed  $\Omega=15.73$  and for two distinct ranges of initial conditions ( $\mathrm{E}[\xi_{0j}^2]$ ). This figure suggests that perturbations of the loads tend to destabilize the system compared to  $\Omega$ , derived for the deterministic case (Section 4.1). Mean-square stability and third-moment stability appear to yield similar results. This result is perhaps not unexpected since the stochastic dynamic equation has a zero diffusion term ( $\mathbf{d_{ae}} = \mathbf{0}$ ) and the stability is mainly controlled by the nonlinear drift functional. Influence of nonlinearity does not seem crucial since a variation in the initial random modal amplitude (Fig. 6a vs. 6b panel) leads to a very similar trend in the MLE.

#### 5. Conclusions

Numerical results suggests that both types of perturbations, if separately considered, can influence the stability and lead to an early exit from the stability domain. Nevertheless, the examined turbulence scenario is rather conservative and perhaps a little unrealistic. Therefore, a loss in turbulence spatial correlation along the blade radius should be considered, i.e., the generalized load could be represented using an equivalent correlation length (less than R). This item will be considered in a future study.

Experimental verification of the findings is also needed. From a practical perspective, future experimental studies may be beneficial as uncertainty in the aeroelastic loads will be quantified, in turn promoting flutter avoidance.

In any case, the study demonstrates that it is possible to formulate the stability problem in a rigorous manner through stochastic differential equations.

#### Acknowledgments

This work was supported in part by the National Science Foundation (NSF) of the United States of America, Award CMMI-1462774. Any opinions, findings and conclusions or recommendations are those of the author and do not necessarily reflect the views of the NSF.

# References

- [1] Lobitz D 2004 Wind Energy 7 211—224
- [2] Hansen M H 2002 Wind Energy 10 551–577
- [3] Pourazarm P, Caracoglia L, Lackner M and Modarres-Sadeghi Y 2015 J. Wind Eng. Ind. Aerodyn. 137 37-45
- [4] Pourazarm P, Modarres-Sadeghi Y and Lackner M 2016 Wind Energy 19 497-514
- [5] Leishman J G 2002 Wind Energy **5** 85–132

doi:10.1088/1742-6596/2647/11/112001

- [6] Resor B and Paquette J 2011 Uncertainties in prediction of wind turbine blade flutter 52nd AIAA/ASME/ASCE/AHS/ASC Structures, Structural Dynamics and Materials Conference AIAA Paper 2011-1947
- [7] Bisplinghoff R, Ashley H and Halfman R 1955 Aeroelasticity (Mineola, NY, USA: Dover Publications Inc.)
- [8] Dowell E H, Clark R, Cox D, Curtiss Jr H C, Edwards J W, Hall Kenneth C, Peters D A, Scanlan R H, Simiu E, Sisto F and Strganac T W 2004 A modern course in aeroelasticity Fourth revised and enlarged edition (Dordrecht, The Netherlands: Kluwer Academic Publishers)
- [9] Jonkman J, Butterfield S, Musial W and Scott G 2009 Definition of a 5-mw reference wind turbine Report Technical Report NREL/TP-500-38060 National Renewable Research Laboratory
- [10] Ernst B and Sueme J R 2013 Modelling structural uncertainty of wind turbine rotor blades for aeroelastic investigations 7th MIT Conference on Computational Fluid and Solid Mechanics
- [11] Pourazarm P, Caracoglia L, Lackner M and Modarres-Sadeghi Y 2016 J. Wind Eng. Ind. Aerodyn. 156 159–171
- [12] Scanlan R H 1997 J. Struct. Eng.-ASCE 123 232-236
- [13] Bucher C G and Lin Y K 1988 J. Eng. Mech.-ASCE 114 2055–2071
- [14] Bucher C G and Lin Y K 1988 J. Fluids Struct.  ${\bf 2}$  437–451
- [15] Lin Y K and Ariaratnam S T 1980 J. Struct. Mech. 8 1–15
- [16] Náprstek J and Pospíšil S 2004 Flutter onset influenced by combined multiplicative and additive random noises Proc. 5th Int. Colloquium on Bluff Body Aerodynamics and Applications (BBAA V) pp 289–292
- [17] Hračov S, Náprstek J and Pospíšil S 2005 Flutter stability condition of bluff body with respect to stochastic approach Proc. 10th Americas Conference on Wind Engr. (10ACWE)
- [18] Lin Y K, Fujimori Y and Ariaratnam S T 1979 AIAA J. 17 545-552
- [19] Fujimori Y, Lin Y K and Ariaratnam S T 1979 AIAA J. 17 673-678 ISSN 0001-1452
- [20] Grigoriu M 2002 Stochastic calculus. Applications in science and engineering (Boston, MA, USA: Birkhäuser)
- [21] Murtagh P J, Basu B and Broderick B M 2005 Eng. Struct. 27 1209–1219
- [22] Burlibaşa A and Ceangà E 2013 Appl. Energy 111 624–635
- [23] Xie W C 2006 Dynamic stability of structures (New York, NY, USA: Cambridge University Press)
- [24] Xie W C and Huang Q 2009 J. Appl. Mech. **76** 031001–10
- [25] Caracoglia L 2022 Stochastic stability of offshore wind turbine blades influenced by rotationally sampled turbulence perturbations *Proc. 2022 Int. Offshore Wind Technical Conference-IOWTC 2022* (ASME) ASME paper IOWTC2022-98201
- [26] Caracoglia L 2021 Stochastic dynamics of rotating wind turbine blades influenced by turbulence and aeroelastic uncertainties: recent developments *Proc. 2021 Int. Mechanical Engineering Congress and Exposition-IMECE 2021* (ASME) ASME paper IMECE2021-73362
- [27] Øksendal B 2003 Stochastic differential equations: an introduction with applications (Berlin-Heidelberg, Germany: Springer-Verlag)
- [28] Li S and Caracoglia L 2019 J. Wind Eng. Ind. Aerodyn. 188 43–60
- [29] Tennekes H and Lumley J 1972 A first course in turbulence (Cambridge, MA, USA: MIT Press)
- [30] Hodges D H and Dowell E H 1974 Nonlinear equations of motion for the elastic bending and torsion of twisted nuniniform rotor blades Report TN D-7818 NASA
- [31] Scanlan R H and Rosenbaum R 1968 Introduction to the study of aircraft vibration and flutter (Dover Publications, New York, New York, USA)
- [32] Bergami L, Gaunaa M and Joachim H 2014 Wind Energy 16 681–693
- [33] Jones R T 1939 The unsteady lift of a finite wing Report Technical Note 682 NACA
- [34] Wong E and Zakai M 1965 Int. J. Eng. Science 3 213–229
- [35] Caracoglia L 2013 Comput. Struct. 122 65–77